Spectral Collapse in Ensembles of Metamolecules

V. A. Fedotov,[1,*] N. Papasimakis,[1] E. Plum,[1] A. Bitzer,[2,3] M. Walther,[2] P. Kuo,[4] D. P. Tsai,[5] and N. I. Zheludev[1,†]

[1]Optoelectronics Research Centre, University of Southampton, SO17 1BJ, United Kingdom
[2]Department of Molecular and Optical Physics, University of Freiburg, D-79104, Germany
[3]Institute of Applied Physics, University of Bern, Sidlerstr. 5, CH-3012 Bern, Switzerland
[4]Institute of Physics, Academia Sinica, Taipei, 11529, Taiwan
[5]Department of Physics, National Taiwan University, Taipei 10617, Taiwan

(Received 5 August 2009; revised manuscript received 20 April 2010; published 1 June 2010)

We report on the first direct experimental demonstration of a collective phenomenon in metamaterials: spectral line collapse with an increasing number of unit cell resonators (metamolecules). This effect, which is crucial for achieving a lasing spaser, a coherent source of optical radiation fuelled by coherent plasmonic oscillations in metamaterials, is linked to the suppression of radiation losses in periodic arrays. We experimentally demonstrate spectral line collapse at microwave, terahertz and optical frequencies.

DOI: 10.1103/PhysRevLett.104.223901 PACS numbers: 41.20.Jb

The burgeoning field of metamaterials provides unique opportunities to engineer the electromagnetic properties of artificial media and achieve exotic functionalities, such as negative refraction and cloaking. Here, we study the dependence of the metamaterial properties on the number of metamolecules in the microwave, THz and optical domain, and demonstrate a new collective phenomenon in metamaterials, where regular ensembles of metamolecules exhibit spectral line collapse.

The reported phenomenon is characteristic of a novel class of artificial media, which we call ''coherent'' metamaterials [1]. An example of a coherent metamaterial is an array of asymmetrically-split rings (ASRs), where the metamolecular excitation corresponds to an oscillating magnetic dipole perpendicular to the plane of the array that does not interact directly with the magnetic field of the incident wave, thus creating a nearly thermodynamically isolated ensemble of strongly interacting coherent ''molecules'' with interesting physical properties. To illustrate this behavior we present a comparison with an ''incoherent'' metamaterial: a two-dimensional array formed by pairs of concentric conducting rings that also supports high-quality resonances. In this case, however, the response of the array is a sum of the individual metamolecule responses, rather than a collective property.

The coherent microwave metamaterial was manufactured as a regular planar array of ASRs etched from a 35 μm thick copper layer on a 1.6 mm thick FR4 substrate. The diameter of the ASR was 6 mm with a line width of 0.4 mm and was split in two segments corresponding to 140° and 160° arcs. The unit cell of 7.5×7.5 mm^2 rendered the arrays nondiffracting at normal incidence for frequencies of up to 40 GHz. In the incoherent metamaterial, ASRs were replaced with pairs of concentric rings. The inner and outer rings had diameters of correspondingly 4.50 mm and 5.45 mm, and were both 0.2 mm wide. The transmission measurements were performed in a microwave anechoic chamber at normal incidence using broadband linearly polarized horn antennas equipped with collimating lenses and a vector network analyzer. The polarization was set parallel to the split in the ASRs.

Transmission spectra of large coherent and incoherent arrays show resonant features in the form of a broad stop-band split by a narrower Fano-like transmission peak (see Fig. 1) which is characteristic of metamaterials with broken symmetry [2,3] and has also been observed in photonic crystal slabs [4,5] and nanoparticles [6]. For the array of ASRs the transmission resonance occurs at around 11 GHz and is associated with the excitation of antisymmetric currents oscillating in the opposite arcs of each split ring (see inset to Fig. 1). Such a current mode, known as a

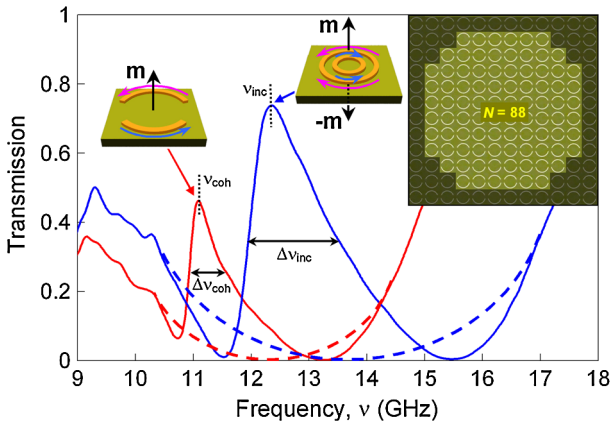

FIG. 1 (color online). Transmission spectra featuring trapped-mode resonances of the coherent (asymmetric split rings, solid red [medium gray] curve, ν_{coh}) and incoherent (concentric rings, solid blue [dark gray] curve, ν_{inc}) metamaterial arrays of 88 metamolecules. Dashed curves indicate transmission stop bands in the absence of trapped-mode excitations. The top right inset shows a sample of 88 metamolecules (unit cells) of the coherent array exposed through a metal mask (represented by the darker area). Other insets show the current modes excited in the unit cells of the coherent (left) and incoherent (right) metamaterials and the corresponding induced magnetic dipole moments m.

trapped or closed mode, yields magnetic dipole moments oriented normal to the array plane, oscillating synchronously (coherently) in all metamolecules. The induced magnetic dipoles interact strongly with one another, while their interaction with the perpendicularly oriented magnetic field of the incident electromagnetic wave is forbidden [2]. For the double-ring metamaterial a similar narrow resonance at 13 GHz corresponds to oscillations of oppositely directed currents in the inner and outer rings, as shown in the inset to Fig. 1. Although such current configurations give rise to magnetic moments, the latter cancel one another leading to a negligible total magnetic moment of the metamolecule. Thus interactions between metamolecules are negligible [7].

Figure 2 shows the dependencies of the transmission resonance quality factors, $Q = \nu/\Delta\nu$ [8], on the total number of metamolecules, N, that form the arrays. In the experiment, the number of metamolecules exposed to the incident wave was controlled by placing metal masks of different sizes on a large metamaterial array, as illustrated in the inset to Fig. 1. These masks screened the peripheral parts of the array, leaving only the central area exposed to electromagnetic radiation. Also, since the masks were in complete contact with the underlying, nonilluminated resonators, the latter were short-circuited and therefore effectively removed from the array so that their presence could not influence the response of the illuminated resonators. The shape of the masks ensured that every unit cell of the array was either fully screened or exposed. These measurements were performed with 22 different masks exposing arrays with a total number of unit cells in the range from 32 to about 700. Experiments with larger arrays were not practical and unnecessary as already for $N \simeq 700$ the quality factor saturated. Experiments with smaller arrays were not feasible as for $N < 32$ diffraction takes its toll on the accuracy of the data. In the measured range of N the experimental data clearly indicate that the Q factor of the coherent metamaterial strongly depends on the size of the illuminated area, i.e., the total number of metamolecules engaged in the interaction with the incident wave. Indeed, the Q factor, which measures about 10.5 for the smallest array ($N = 32$), can be seen to increase by almost 70% reaching 17.5 for the full-sized array with $N = 688$. In contrast, the Q factor of the incoherent metamaterial appears to be practically independent of the number of exposed unit cells and remains at around $Q = 9$.

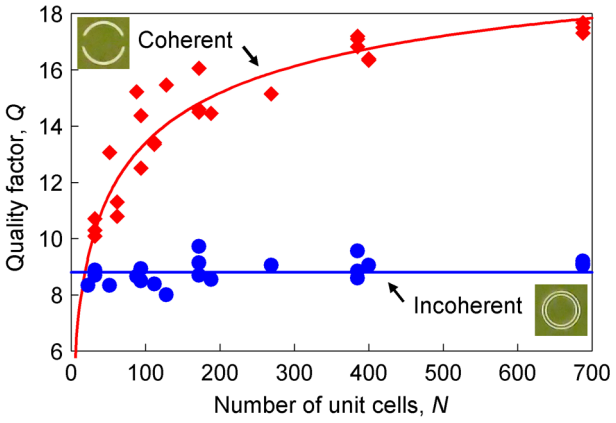

FIG. 2 (color online). Q-factor as a function of the total number of metamolecules. Experimentally measured data are represented by points for both coherent (diamonds) and incoherent (circles) metamaterials. Solid lines present theoretical fits to the data.

To illustrate further the dependence of the resonant response on the size of the coherent metamaterial, we compared the excitation of a single isolated ASR to that of a large array containing $N = 400$ unit cells. As transmission and reflection measurements of a single metamolecule are not realistic, it is more practical to look for signatures of the trapped-mode excitation in the near field of the ASR. Since there is practically no difference between the responses of THz and microwave metamaterials, we studied the spatial distribution of the magnetic field using a state-of-the-art THz near-field imaging technique resolution described in [9] (see supplementary material [10]). For this we fabricated THz versions of the metamaterial structures, which corresponded to the original ASR scaled down by about 13 times. The technique enabled accurate mapping of the electric field $\vec{E}$ in the plane of the unit cell (as illustrated in the inset to Fig. 3(a)), which was used to calculate the z component of the magnetic field $\vec{H}$ via the Maxwell equation $\vec{\nabla} \times \vec{E} = -\mu \partial \vec{H}/\partial t$.

We observed that at resonance conditions the spatial distribution of the magnetic field was radically different for a split ring placed in the array and an isolated split ring. For a ring in the array, the magnetic field penetrates the unit cell in the same direction everywhere within the area enclosed by the ring: the total magnetic moment of the metamolecule is at maximum indicating the excitation of strong antisymmetric (i.e., ring) currents in opposite sections of the ring [see Fig. 3(b)], while the spectral dependence of the squared amplitude of the magnetic flux reveals a narrow sharp peak centered at $\nu_1 = 0.165$ THz [see Fig. 3(a)]. For an isolated single metamolecule, the net magnetic flux is also nonzero but it is much lower than for a ring in the array: the magnetic field is oppositely directed in adjacent sections of the ring [see Fig. 3(c)], the total magnetic flux is small and the antisymmetric current component is weak. As a result, the resonant feature at $\nu_2 = 0.142$ THz is much less pronounced and its Q factor is significantly lower than for rings in the array indicating considerable damping [see Fig. 3(a)].

We attribute the observed size-dependent resonant response of the coherent metamaterial to the existence of strong interactions between the metamolecules mediated by magnetoinductive surface waves [11]. The latter are produced by magnetic dipoles coherently oscillating perpendicular to the array plane, which in the case of a regular infinite (or very large) array, reradiate only in the plane, as follows from symmetry considerations. Such surface

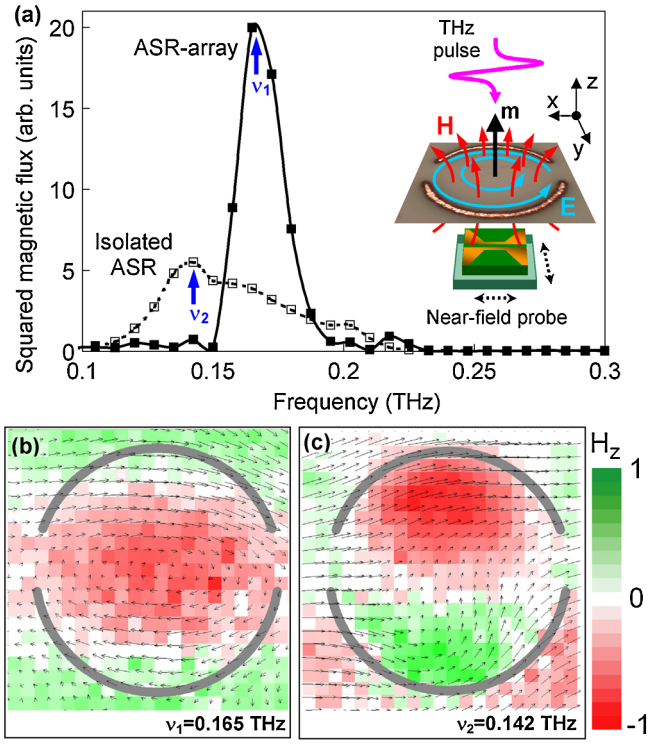

FIG. 3 (color online). Panel (a) shows the spectral dependence of the squared total magnetic flux amplitude through an ASR for the cases of one isolated ring (empty squares) and a ring located in the middle of a 20×20 array (filled squares). Panels (b) and (c) present snapshots of the instantaneous magnetic field normal to the plane of the ring (color coded) and the in-plane electric field (arrows) at resonance frequencies ν_1 and ν_2 correspondingly. To show both fields at their maxima on the same map the magnetic and electric fields are presented with a phase shift of $\pi/2$. The inset shows the experimental configuration for the THz near-field scans. A near-field probe is raster scanned behind the sample illuminated by a THz pulse.

waves may only scatter at the edges of the structure, thus efficiently trapping electromagnetic energy and ensuring a high Q factor of the system. The scattering losses grow and the Q factor diminishes as the array becomes smaller, and in the limiting case of an isolated metamolecule the resonance is weak due to scattering losses through magnetic dipole radiation.

The dependence of the Q factor on the size of the array can be qualitatively understood from the definition of the Q factor, $Q = 2\pi(E/\Delta E)$, where E is the energy stored in the array and ΔE is the energy dissipated by the array per cycle. Here E is simply proportional to N, while $\Delta E = \Delta E_m + \Delta E_s$ represents contributions from two loss mechanisms. $\Delta E_m = \sigma_m N$ includes material losses, i.e. Ohmic losses in the metal and dissipation losses in the dielectric substrate, as well as radiation losses due to an electric dipole induced in each unit cell (controlled by the degree of asymmetry). Losses associated with scattering of the magnetoinductive waves on the edges of the array, ΔE_s, are proportional to the length of its perimeter and thus $\Delta E_s = \sigma_s\sqrt{N}$. Thus, the phenomenological dependence of the quality factor on the number of unit cells can be presented in the form $Q \propto N/(\sigma_m N + \sigma_s\sqrt{N})$, which fits the experimental data very well (solid red [medium gray] line in Fig. 2). In comparison, in the case of incoherent arrays (concentric pairs of rings) the total induced magnetic moment in each unit cell is small; hence, magnetic dipole interactions and scattering of magnetoinductive waves are negligible ($\sigma_m N \gg \sigma_s\sqrt{N}$). The second term in the denominator can be disregarded making the Q factor independent of the size of the array, which is in complete agreement with our experimental observations (solid blue [dark gray] line in Fig. 2). It is important to note here that the size effect cannot result from the well-known mechanism of diffraction at the edges of the finite-size array, where scattered waves with non-normal wave vectors may couple to the array's surface modes and thus affect the strength of the resonant intermolecular interaction. Such situation would be equivalent to illuminating the array with a mixture of waves at different angles of incidence. Our experiments (see supplementary material [10]), however, indicate that the angular dependence of the trapped-mode resonance in the ASR array is very weak and thus the diffraction mechanism cannot account for the observed strong size effect. Furthermore, weak angular dependence similar to that of the ASR array was also found in the case of incoherent metamaterial composed of concentric rings [7], but the absence of any measurable dependance on the array size suggests that the contribution of the diffraction coupling mechanism to the size effect, if present, is exceptionally small. Finally, the diffraction mechanism fails to explain the absence of the trapped-mode resonance in the case of a single ASR demonstrated both in the microwave [1] and in the THz part of the spectrum (Fig. 3).

The dependence of the resonant response on the array's size results from truly classical interactions between the excited states of the metamolecules and therefore shall be scalable with wavelength. Since the characteristic array size at which substantial broadening of the resonance occurs corresponds to $N = (\sigma_s/\sigma_m)^2$, with increase of Joule losses the size effect will be seen in smaller arrays, i.e., in an array with higher Joule losses the coherent state will be formed by a smaller number of metamolecules.

This is exactly what we observed in our experiments in the optical part of the spectrum, where Joule losses are dominant. Here we studied transmission of square asymmetric split ring slit arrays of different sizes scaled down 15 000 times relative to the microwave sample. The ring slits (complimentary to split rings) were cut from a 55 nm thick gold film supported by a 500 μm silica substrate using focused ion beam milling. The transmission measurements were performed using a microscope-based spectrophotometer. We studied arrays of five different sizes containing from 16 to 144 metamolecules [see Figs. 4(a) and 4(b)]. Such photonic metamaterials exhibited a trapped-mode resonance at around 1000 nm, which, in

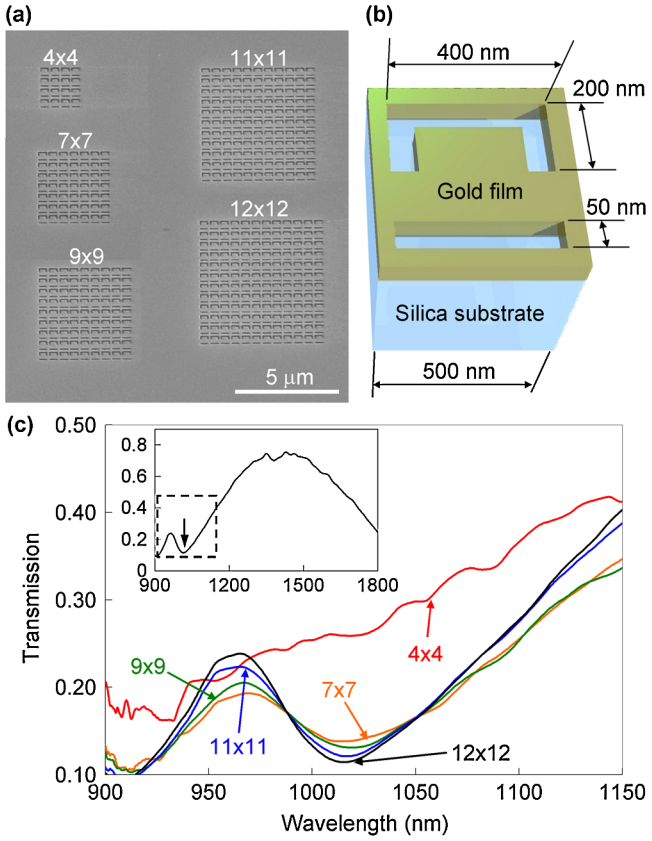

FIG. 4 (color online). (a) Scanning electron microscopy images of coherent metamaterial arrays of different sizes. (b) Schematic of the metamaterial unit cell. (c) Transmission spectra of the metamaterials in the vicinity of the trapped-mode resonance. Inset to (c): spectrum of the 12×12 array over a much wider wavelength range; a dashed box indicates the spectral domain that is covered by the main plot, while an arrow marks the resonance.

accordance with Babinet's principle [12,13], was seen not as a transmission peak (as for a *positive* array, see Fig. 1), but as a dip in transmission for the largest array of 12×12 unit cells [see inset to Fig. 4(c)]. For smaller arrays the resonance gradually became broader and shallower and, as shown in Fig. 4(c), completely disappeared for $N = 16$, which suggests that the most dramatic change occurs when the number of unit cells drops below 49. However, the observed size effect at optical frequencies cannot be attributed only to the increased radiation losses of smaller arrays. Indeed, the contribution of the trapped-mode radiation losses to size effect is much weaker due to the increased dissipation in the metal. As such we expect a significant contribution from the presence of non-normal wave vectors due to the finite array size.

The results presented above illustrate that larger arrays of coherent metamaterials exhibit narrower resonances. They also show that in samples with smaller losses more metamolecules are engaged in forming the coherent state: the Q factor starts reducing dramatically below about 200 metamolecules in the microwave array, while in the lossy optical case we saw a significant reduction of Q factor below 49 metamolecules. We argue that the number of molecules forming the coherent response will increase as Joule and dielectric losses are reduced. This is relevant to the recent observation of loss compensation in a coherent photonic metamaterial [14], which paves the way to an intriguing opportunity of creating a lasing spaser, a coherent source of optical radiation fuelled by coherent plasmonic oscillations in individual metamaterial resonators of a coherent array. In the latter case, the gain substrate supporting the rings would be the source of energy [15].

The authors acknowledge the financial support of the Engineering and Physical Sciences Research Council, U.K., the Royal Society, and the European Community project ENSEMBLE.

*vaf@orc.soton.ac.uk
†www.nanophotonics.org.uk/niz

[1] N. Papasimakis, V. A. Fedotov, Y. H. Fu, D. P. Tsai, and N. I. Zheludev, Phys. Rev. B **80**, 041102(R) (2009).
[2] V. A. Fedotov, M. Rose, S. L. Prosvirnin, N. Papasimakis, and N. I. Zheludev, Phys. Rev. Lett. **99**, 147401 (2007).
[3] A. Chirst *et al.*, Nano Lett. **8**, 2171 (2008).
[4] S. Fan and J. D. Joannopoulos, Phys. Rev. B **65**, 235112 (2002).
[5] N. A. Gippius, S. G. Tikhodeev, and T. Ishihara, Phys. Rev. B **72**, 045138 (2005).
[6] Y. Wu and P. Nordlander, J. Chem. Phys. **125**, 124708 (2006).
[7] N. Papasimakis *et al.*, Appl. Phys. Lett. **94**, 211902 (2009).
[8] A full characterization of the observed resonances requires taking into account their asymmetric Fano profile [3], which we reserve for a future work.
[9] A. Bitzer, H. Merbold, A. Thoman, T. Feurer, H. Helm, and M. Walther, Opt. Express **17**, 3826 (2009).
[10] See supplementary material at http://link.aps.org/supplemental/10.1103/PhysRevLett.104.223901.
[11] E. Shamonina, V. A. Kalinin, K. H. Ringhofer, and L. Solymar, J. Appl. Phys. **92**, 6252 (2002).
[12] T. Zentgraf *et al.*, Phys. Rev. B **76**, 033407 (2007).
[13] Although Babinet's principle is not strictly valid in the optical domain, it can be employed to explain, at least qualitatively, the main spectral features of complementary split-ring arrays as shown in [12].
[14] E. Plum, V. A. Fedotov, P. Kuo, D. P. Tsai, and N. I. Zheludev, Opt. Express **17**, 8548 (2009).
[15] N. I. Zheludev, S. L. Prosvirnin, N. Papasimakis, and V. A. Fedotov, Nat. Photon. **2**, 351 (2008).